

Multifractal Analysis of Microvasculature in Health and Disease

Wil O. C. Ward, Li Bai

Abstract—A growing body of evidence suggests that there is a strong association between neurodegenerative diseases such as Alzheimer’s Diseases and the abnormality of the cerebral vasculature, in particular the microvessels/capillaries that are responsible for the exchange of nutrients across the blood-brain barrier [1]. Many microvessels are described as being kinked or distorted [2], implying that they are modified by some destructive process. Imaging devices such as microCT can achieve resolutions on the order of several μm , allowing imaging the three dimensional (3D) microvasculature down to the capillary level. However, the main weakness of using microCT for vascular research is considered to be the lack of software for 3D quantification of microvasculature and microvascular image databases for developing and testing algorithms.

In this paper we describe a multifractal analysis method for the microvasculature automatically segmented from microCT images of the mouse brain. Due to the lack of a benchmark microCT image database, the method has been tested using a surrogate database - a publicly available retinal vessel database. The results are preliminary indication of the multifractal properties of mouse brain vasculature. A potential solution to automated classification of healthy and disease brains are discussed.

Index Terms—multifractals, sandbox method, retinal analysis, microvasculature, microCT

I. INTRODUCTION

FRACTALS can be described as objects which contain regions that are in a way similar to the object as a whole. They are found in many natural scenarios, from financial time series to quantum mechanics, and in particular in many areas of human physiology [3], [4]. Each fractal has particular non-integer dimension that represents how objects fill in the space. A generalisation of this dimension is the theory of multifractal systems [5], in which objects exhibit varying fractal dimensions that form a continuous fractal spectrum.

It has previously been found that the structure of blood vessels in the human retina displays these fractal properties [6], [7], [8], [9]. Using this information, it can be shown that different levels of pathological deterioration affect the multifractal spectrum, and thus it can be used as a property with which to classify images [6], [7], [8].

This paper describes a multifractal microvascular analysis method, which is part of the ongoing research that looks into automated segmentation and analysis of the three-dimensional (3D) vasculature from images of the mouse brain obtained through the application of microCT and resin

casting. The method developed is tested on automatically segmented retinal vasculatures from the STARE retinal vessel database, which contains information on whether the patient suffers from pathological degeneration [10]. The retinal vessel database is used in this work as a surrogate, as presently no publicly available database of microvasculature exists. The automated retinal segmentation method is described in section II-B.

II. THEORY AND DESIGN

A. Multifractal Spectrum Analysis

When assessing a particular signal, common points of interest are the presence of singularities, where the signal is irregular or discontinuous at a point. One characteristic of a singularity’s strength is the Hölder exponent. For a distribution f , if the following condition exists

$$|f(\mathbf{x}) - P_n(\mathbf{x} - \mathbf{x}_0)| \leq C |\mathbf{x} - \mathbf{x}_0|^h$$

for some polynomial P_n , with degree $n < h$, then the supremum of all $h \in (n, n + 1)$ where it holds is called the Hölder exponent $h(\mathbf{x}_0)$ of singularity \mathbf{x}_0 . The exponent here represents a local analysis of regularity in the signal. Calculating this singularity spectrum involves finding the set of all points with the same Hölder exponents, $\mathcal{S}(h)$, within the signal. The spectrum, $D(h)$, is a function of $\mathcal{S}(h)$.

A common method for calculating fractal dimensions is the box counting method [3]. This is implemented by placing a grid of boxes with decreasing dimension, ε , over the whole signal and counting the number of boxes, $N(\varepsilon)$, containing any part of the structure being analysed. This number is expected to scale with the box dimension, since $N(\varepsilon) \sim \varepsilon^{-D}$, where D is the fractal dimension of the signal, allowing the dimension to be calculated as the gradient of a linear regression plot fit to $\log(1/\varepsilon)$ against $\log(N(\varepsilon))$.

This method, however, is not suited to calculating multifractals, so a different approach is used, utilising the box dimension’s relation with the fractal dimension [5]. This method involves placing boxes at random points on the structure and increasing the box dimension. The results are then compared at each size with the respective signal found at other locations. In the case of 2-dimensional images, the signal becomes a structure, with mass M_0 : the image dimension is given by L . For some continuous infinite set of arbitrary exponents, Q , the generalized fractal dimension D_q

Manuscript received 11/04/2013

Wil Ward and Li Bai are with the School of Computer Science, University of Nottingham, Nottingham, UK

(email: wil.oc.ward@gmail.com, bai@cs.nott.ac.uk)

is defined as follows:

$$\sum_{i=1}^N \left(\frac{M_i}{M_0} \right)^Q \sim \left(\frac{l}{L} \right)^{(Q-1)D_Q},$$

where M_i is mass of the structure contained in the i^{th} box of dimension l , and N is the maximum possible number of boxes. Here Q is used to distort the structure, allowing the focused analysis on different fractal properties [5].

Adapting this equivalence to a discrete image involves taking an appropriate finite set of exponents and approximating the signal on a finite number of boxes. For some N_0 finite number of boxes with increasing dimension r , the average spatial quantity for a box at a distortion exponent is:

$$\bar{m}_q(r) = \frac{1}{N_0} \sum_{i=1}^{N_0} \left[\left(\frac{M_i(r)}{M_0} \right)^{q-1} \right]$$

$M_i(r)$ represents the mass of structure contained in the box of dimension r in the i^{th} position. Using the above equivalence relation, D_q can be approximated at $Q = q$ using \bar{m}_q :

$$D_q \propto \frac{1}{q-1} \left(\frac{\log \bar{m}_q(r)}{\log r - \log L} \right)$$

This allows the dimension for each exponent to be calculated as the gradient of a linear regression fit of the function $\log(\bar{m}_q(r))/(q-1)$ against $\log(r/L)$, $\forall r$ [5].

The spectrum of D_q against q is a representation of a continuous monotonically decreasing function, that should yield a linear plot for monofractals. Using D_q , the local Hölder exponent, α , and its corresponding dimension spectra $D(\alpha)$ can be found. This is a commonly used spectrum in literature, [4], [6], [8], [5], [11], and is equivalent to the notation $f(\alpha)$. First, define

$$\begin{aligned} \tau(q) &= (q-1)D_q, \\ \alpha(q) &\cong \frac{d\tau(q)}{dq} \end{aligned}$$

and apply the Legendre transform, which defines the relationship between $\tau(q)$ and $D(\alpha)$:

$$D(\alpha) = q\alpha(q) - \tau(q)$$

In theory, an infinite number of exponents q should lead to α_{\max} and α_{\min} , the limits of α that form the support of $D(\alpha)$ [12]. The spectrum of a multifractal should peak such that $\max_{\alpha} D = D(\alpha_0)$, $\alpha_0 \equiv \alpha(q=0)$. This is representative of the monofractal dimension [3].

Figure 1 shows an example of the boxes used to count the 2D signal at three random points. There is also an example of the τ function for the counts, plotted against the exponents Q . Note that the largest box for a particular location does not exceed the boundaries of the images, so as not to distort the results. Where there is no count for a certain dimension, \tilde{r} , for that location the image is not included in the calculation $\bar{m}_q(\tilde{r})$. This does not exempt it from the average at lower box dimensions.

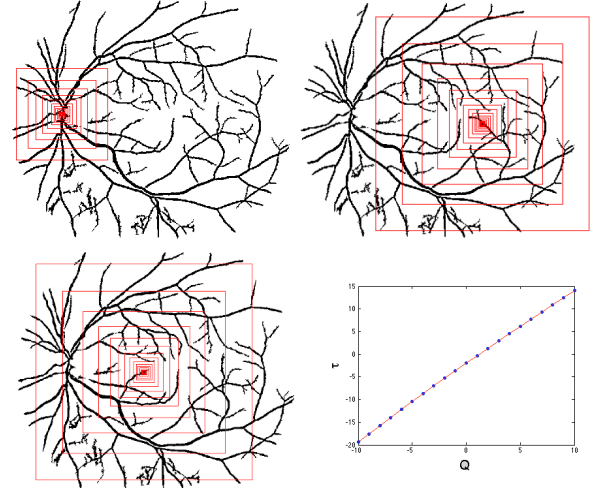


Figure 1. Sandbox counting for multifractal analysis at 3 separate locations on the vessel structure of im0162 and average $\tau(q)/q$ plot

B. Segmentation Algorithm

To prepare images for fractal analysis, vessels must first be identified and presented as a binary representation. Previous work uses manual segmentations but this work uses an automated detection algorithm to obtain vessels. Existing methods were reviewed [13], [14], [15], that use a variety of approaches to segmentation, however for retinal images, many did not identify areas of bright diabetic retinopathic (DR) lesions that are present in many of the pathological images in our dataset. The need to remove these lesions is necessary to get a good approximation of the fractal dimensions of vessels, and with many current segmentation methods it is difficult to distinguish the tear-like edges from vessel structures.

The two major steps of the segmentation framework are detection of vessel-like objects, and background profile generation [16]. The former applies thresholding to the numerical divergence at each pixel in the image. Following this a linear morphological operator is applied about several rotations to isolate linear structures. To create an initial background profile, all pixels within a small deviation of the image median intensity are isolated. This removes vascular structure and DR lesion alike, allowing a background for these regions to be interpolated using true background pixels. Identified vessel-like structures from the first step are compared with their corresponding background profile, and if their original intensity is significantly lower than the approximate background of the same region, this structure is considered to be a true vessel. All other structures are discarded from the mask, including areas of high colour intensity, and the remaining structure is used as the binary vessel mask.

To increase contrast between vessels, the green channel of the retinal images was used, as red vessels show up very dark in the grey-scale image. In the case of the mouse brain image where bright lesions are not present, the background profiling

Pathological			Healthy		
Patient	Auto	Stošić	Patient	Auto	Stošić
im0001	1.5472	1.5840	im0077	1.6490	1.6670
im0002	1.4415	1.5740	im0081	1.6028	1.6590
im0003	1.5312	1.5950	im0082	1.6173	1.6680
im0004	1.3919	1.5730	im0162	1.6371	1.6790
im0005	1.6391	1.5730	im0163	1.6264	1.7140
im0044	1.6002	1.6800	im0235	1.6251	1.6850
im0139	1.5838	1.6660	im0236	1.6166	1.6830
im0291	1.5509	1.6030	im0239	1.5967	1.6580
im0319	1.3630	1.5540	im0240	1.5514	1.6560
im0324	1.5360	1.6440	im0255	1.5986	1.6560
Mean	1.5185	1.6046	Mean	1.6121	1.6725

Table I

CAPACITY DIMENSION, $D(\alpha_0)$, OF STARE DATABASE IMAGES USING THE SANDBOX COUNTING FOR CALCULATING MULTIFRACTAL SPECTRA, INCLUDING THE RESULTS FROM STOŠIĆ AND STOŠIĆ ON MANUAL SEGMENTATION USING THE SANDBOX METHOD

was obsolete and not included as a step in the segmentation process. To conform with the properties of grey-scale retinal images, the mouse brain image was inverted into negative, so that vasculature is a dark mass.

Accuracy, true positive rate and false positive rate when compared to the ground truth are presented below. Sensitivity is equivalent to the rate of true positives and specificity is equivalent to 1 minus the rate of false positives. This compares favourably with other unsupervised segmentation methods.

Accuracy	Sensitivity	Specificity
0.9496	0.8050	0.9686

III. RESULTS

After obtaining segmentations of the vessels from retinal images and the microvasculature, the sandbox dimension counting method was applied to both datasets, to calculate the multifractal spectra of all images. In the case of retinal vessels, the binary masks were padded with zeros in such a way that it would form an N -by- N square image, where N is the length of the largest dimension of the original image. This was for consistency in computation due to the scaling of square boxes.

A. Parameters

For this method, the set of exponents, q , for which to estimate the continuous set of exponents, Q , was set as $[-10, 10] \subset \mathbb{Z}$. For $q = 1$, D_q is undefined and so a finite difference estimate was used by taking $D_{q=1} \approx (D_{q=1-\epsilon} + D_{q=1+\epsilon})/2$, for $\epsilon = 0.001$.

The number of boxes used was $N_0 = 1000$, width increasing dimension at a ratio of $\frac{4}{3}$, centred at random points on the vessel structure. This process was repeated 100 times (for different sets of 1000 random points) and the result averaged. The parameters match those used in the implementation by Stošić and Stošić [8].

B. Multifractal Spectra

Numerical results from the application on the retinal vasculature shows a distinct difference in dimension between

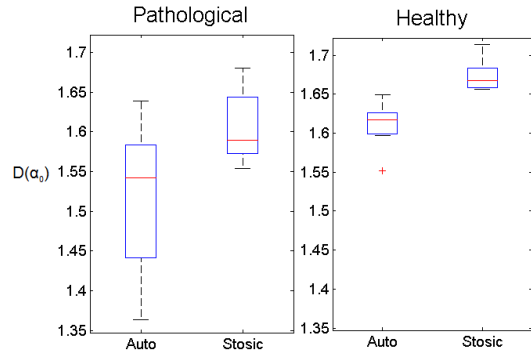


Figure 2. Boxplot illustrating the data in Table I. This shows both the distinct difference between dimensions of pathological and healthy retina as well as highlighting the effects of using an automated approach to segmentation

the healthy and pathological patients. Figure 3 shows that both datasets exhibit similar shape, however the pathological plot is shifted with lower values for all $\alpha(q)$ and $D(\alpha)$, when compared with the spectrum of healthy patients. This matches the results found by Stošić and Stošić in the analysis of manual segmentations of the same dataset [8] as seen in Figure 2. Minor difference between the two sets of results can be put down to both the random element of the method, and due to detection errors in the segmentation framework. In general, there is good grounds for automated classification and registration using the results presented here, as the distinct variation between spectra of healthy and unhealthy retina can reduce the problem of classification into a smaller dimension of individual spectra.

The results from application to a mouse brain image, shown in Figure 4, are shown in Figure 5 and illustrate that it too exhibits multifractal properties. Creating a database of 3D microvasculature of mouse and rat brains using microCT imaging is currently ongoing work. The multifractal properties of this kind of structure could lead to classification solutions (similar to those identified in the retinal dataset) of healthy brains and those with Alzheimer’s disease which causes angiogenesis, giving a more complex vascular system [1].

IV. DISCUSSION

The multifractal analysis framework presented here could similarly be applied to 3D datasets, by extending the 2D boxes to volumetric structures and scaling on a set of random points. This approach would be expensive in terms of computation runtime, as the sandbox method is relatively inefficient. The need for a large number of box locations and repeated applications to get significant coverage of the data, coupled with the increase in data points for higher dimension data, reduces the viability of sandbox method for the analysis. Other approaches to determining the multifractal spectra would improve computing performance and accuracy. An example of this is to use wavelet analysis of the signal: the multiscale property of wavelets would allow the use of

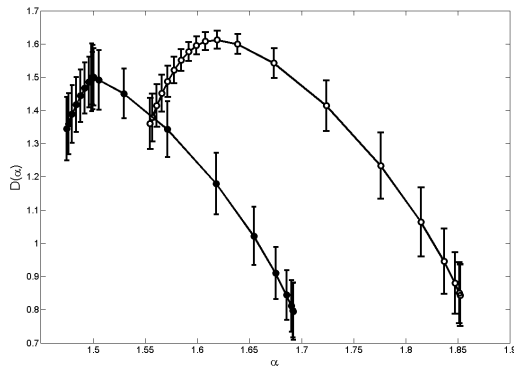


Figure 3. Mean multifractal dimension spectra for retinal image dataset, showing difference in dimensions between healthy and pathological retina. Healthy patients are represented by the curve with open circles, pathological with solid circles [Vertical error bars show ± 1 standard deviation]

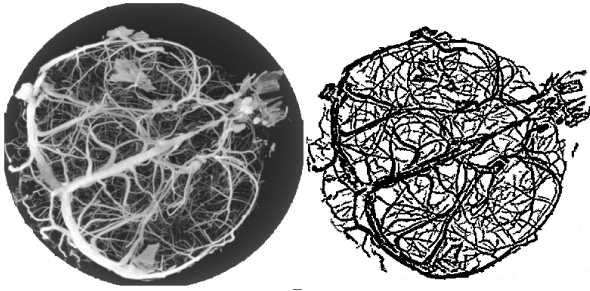


Figure 4. 2D representation of mouse brain microCT scan and its microvasculature mask, segmented using the automatic method presented

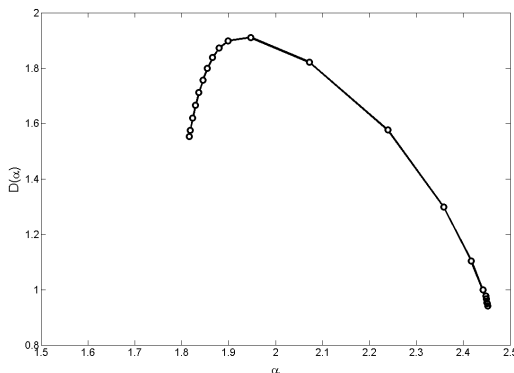


Figure 5. Dimension spectra of mouse brain segmentation in Figure 4 exhibiting multifractal properties. Dimension and Hölder exponents are higher than those of retinal vessels due to increased complexity in vasculature

a single transform to analyse the entire data and remove the requirement for repeated applications. However the theory and implementation are less straightforward when compared with the sandbox method. This approach has been used on 1D signals [17].

Results shown here on the retinal vessels complement the idea that multifractal spectra could be used to characterise

the microvasculature for automated clinical diagnosis using machine learning methods. The analysis results of the mouse brain microCT images further reinforce the use of such techniques. The available of large microCT datasets of the microvasculature of varying state of health would allow more extensive analysis on to clarify further the suitability of multifractal analysis as a valuable tool for microvascular disease classification.

REFERENCES

- [1] R. Weller, D. Boche, and J. Nicoll, "Microvasculature changes and cerebral amyloid angiopathy in alzheimer's disease and their potential impact on therapy," *Acta Neuropathol*, vol. 118, no. 1, pp. 87–102, 2009.
- [2] V. T. Marchesi, "Alzheimer's dementia begins as a disease of small blood vessels, damaged by oxidative-induced inflammation and dys-regulated amyloid metabolism: implications for early detection and therapy," *The FASEB Journal*, vol. 25, no. 1, pp. 5–13, 2011.
- [3] G. A. Losa, "Fractals in biology and medicine," in *Encyclopedia of Molecular Cell Biology and Molecular Medicine*. Wiley, 2011.
- [4] L. Yu and D. Qi, "Holder exponent and multifractal spectrum analysis in the pathological changes recognition of medical CT image," in *Control and Decision Conference*, Mianyang, China, 2011.
- [5] T. Tel, A. Fulop, and T. Vicsek, "Determination of fractal dimensions for geometrical multifractals," *Physica*, vol. A, no. 189, pp. 155–166, 1989.
- [6] A. Avakian, R. E. Kalina, E. H. Sage, A. H. Rambhia, K. E. Elliott, E. L. Chuang, J. I. Clark, J.-N. Hwang, and P. Parsons-Wingert, "Fractal analysis of region-based vascular change in the normal and non-proliferative diabetic retina," *Current Eye Research*, vol. 24, no. 4, pp. 274–280, 2002.
- [7] M. Z. C. Azemin, D. K. Kumar, T. Y. Wong, J. J. Wang, P. Mitchell, R. Kawasaki, and H. Wu, "Age-related rarefaction in the fractal dimension of retinal vessel," *Neurobiology of Aging*, no. 33, pp. 194.e1–194.e4, 2012.
- [8] T. Stosic and B. D. Stosic, "Multifractal analysis of human retinal vessels," *IEEE Transactions on Medical Imaging*, vol. 25, no. 8, pp. 1001–1007, 2006.
- [9] S. Talu and S. Giovanzana, "Image analysis of the normal human retinal vasculature using fractal geometry," *Human and Veterinary Medicine Bioflux*, vol. 4, no. 1, pp. 14–18, 2012.
- [10] A. Hoover, V. Kouznetsova, and M. Goldbaum, "Locating blood vessels in retinal images by piece-wise threshold probing of a matched filter," *IEEE Transactions on Medical Imaging*, vol. 19, no. 3, pp. 203–210, 2000.
- [11] R. Lopes and N. Betrouni, "Fractal and multifractal analysis: A review," *Medical Image Analysis*, no. 13, pp. 634–649, 2009.
- [12] B. R. Masters, "Fractal analysis of the vascular tree in the human retina," *Annual Review of Biomedical Engineering*, no. 6, pp. 427–452, 2004.
- [13] F. Zana and J.-C. Klein, "Segmentation of vessel-like patterns using mathematical morphology and curvature evaluation," *IEEE Transactions on Image Processing*, vol. 10, no. 7, pp. 1010–1019, 2001.
- [14] J. Hajer, K. Hamrouni, and E. Noureddine, "Blood vessels segmentation in retina image using mathematical morphology and the stft analysis," in *XIV Brazilian Symposium on Computer Graphics and Image Processing*, 2001.
- [15] B. S. Y. Lam and H. Yan, "A novel vessel segmentation algorithm for pathological retina images based on the divergence of vector fields," *IEEE Transactions on Medical Imaging*, vol. 27, pp. 237–246, 2008.
- [16] C. Kose, U. Sevik, C. Ikibas, and E. Hidayet, "Simple methods for segmentation and measurement of diabetic retinopathy lesions in retinal fundus images," *Computer Methods and Programs in Biomedicine*, no. 107, pp. 274–293, 2012.
- [17] A. Holdsworth, N.-R. Kevlahan, and D. J. Earn, "Multifractal signatures of infectious diseases," *Journal of the Royal Society Interface*, no. 9, pp. 2167–2180, 2012.